IEEE Photonics Journal
An IEEE Photonics Society Publication

Design of Low-loss and Highly Birefringent Porous-Core Photonic Crystal Fiber and Its Application to Terahertz Polarization Beam Splitter

Volume 10, Number 4, August 2018

E. Reyes-Vera
J. Úsuga-Restrepo
C. Jiménez-Durango
J. Montoya-Cardona
N. Gómez-Cardona

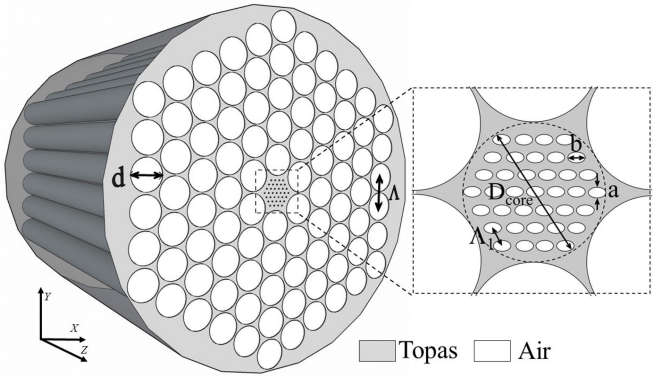

DOI: 10.1109/JPHOT.2018.2860251
1943-0655 © 2018 IEEE

IEEE photonics SOCIETY
IEEE

Design of Low-loss and Highly Birefringent Porous-Core Photonic Crystal Fiber and Its Application to Terahertz Polarization Beam Splitter

E. Reyes-Vera, J. Úsuga-Restrepo, C. Jiménez-Durango, J. Montoya-Cardona, and N. Gómez-Cardona

Department of Electronic and Telecommunications Engineering, Instituto Tecnológico Metropolitano, Medellín 050013, Colombia

DOI:10.1109/JPHOT.2018.2860251

Manuscript received July 4, 2018; accepted July 21, 2018. Date of publication July 26, 2018; date of current version August 7, 2018. This work was supported by Instituto Tecnologico Metropolitano under projects P15108 and P17127. The work of J. Úsuga-Restrepo was supported by Instituto Tecnolgico Metropolitano through the program Young Researchers 2017. The work of J. Montoya-Cardona was supported by Instituto Tecnolgico Metropolitano through the program Young Researchers 2018.This paper was presented in part at the Third International Conference on Applications of Optics and Photonics, Faro, Portugal, May 2017. Corresponding author: E. Reyes-Vera (e-mail: erickreyes@itm.edu.co).

Abstract: We present the design of a porous-core PCF with elliptical holes in the core that achieved low loss, high birefringence, and flattened dispersion for guiding terahertz waves. The finite element method is used to study the properties of the designed waveguide in detail: effective material loss, birefringence, confinement losses, and dispersion. Simulation results show that the proposed structure exhibits simultaneously high modal birefringence of 1.32×10^{-2} and a flattened dispersion over a broadband of 1.28 THz. Then, polarization splitters, based on both symmetric and asymmetric porous-core PCF structures, are designed and evaluated at 1 THz. We show that this kind of device exhibits a strong polarization-dependent coupling behavior. Numerical results show that the configuration based on dual-core waveguide with asymmetric cores can achieve a 10.9 cm long splitter with a broadband of 0.306 THz for *x*-polarization and 0.23 THz for *y*-polarization. Finally, this paper offers an effective method to design an ultrawideband polarization beam splitter to operate in the THz region, which might be relevant for future applications in technical areas, such as spectroscopy, sensing, and high-speed data transmission.

Index Terms: Photonic crystal fibers, fiber optics devices, terahertz wave, terahertz polymer fiber, polarization splitter, polarization-selective devices.

1. Introduction

Terahertz radiation band is the portion of the electromagnetic spectrum from 0.1 THz to 10 THz. This region of the spectrum has received substantial attention due to the great interest in a large range of technical areas, such as diagnostic imaging [1], [2], spectroscopy [3]–[5], gaseous sensing [4], [6] and high-speed data transmission [7]. However, most of THz devices use air to propagate the waves. Thus, when the radiation propagates in free space, the waves experience many hazards, including scattering, diffraction, and transmitter-receiver alignment problems [3], [8]. In addition, the THz waves can experiment high absorption losses because the THz radiation is strongly absorbed by the

steam present in the surrounding medium. In order to solve these problems, researchers proposed waveguides instead of free space transmission. In the last decade, THz waveguides have undergone a series of changes in the research area. The first configurations of THz waveguides were based on parallel-plates [9], bare metal wires [10], terahertz pipe waveguides [11] and traditional microwave waveguides [12], but all of them presented high confinement losses. Thus, the next logical step was to use waveguides made up of dielectric materials, since these materials show obvious advantages compared with the metallic ones, e.g., it does not have ohmic losses and it uses flexible materials. However, most of dielectric materials also have a high absorption loss in the THz region. Hence, to suppress the material absorption in a THz waveguide design, the key strategy is to maximize the fraction of power guided in dry air, which is almost transparent in the THz frequency range [13]. Then, a new kind of waveguides based on polymer Photonic Crystal Fibers (PCF) were explored because the air-hole lattice structure provides an additional degree of freedom and offers different properties of wave propagation. This type of fibers offers the possibility of controlling properties, such as dispersion, birefringence, and losses through the variation of its geometric parameters [14]–[18].

On the one hand, several waveguides have been proposed based on polymer PCFs, such as subwavelength plastic fibers [19], hollow core fibers [20], [21], honeycomb PCF [22], among others. A more promising configuration is based on sub-wavelength porous-core, which has some advantages, such as extremely low material absorption loss, small core diameters, low dispersion, and larger bandwidth compared with hollow core fibers [15]–[17]. These properties are better than in conventional PCFs because the sub-wavelength diameter of the holes in the core region helps to confine the modes within smaller air holes surrounded by the large air cladding. Several porous core configurations have been reported in the past. The porous core PCFs were introduced for the first time in 2008 by Atakaramians *et al.* [23]. That work studied the physics of the THz waves propagating in a porous-core fiber and analyzed the porosity as a key factor in this type of structures. One year later, the same research group demonstrated that the fabrication of a highly porous THz Fiber with symmetrical and asymmetrical sub-wavelength air-holes is possible and, they validated the low dispersion characteristics of the porous fibers [24]. Afterward, in 2011 Nielsen *et al.* [25] analyzed a photonic band-gap fiber with honeycomb porous-core and demonstrated that this type of core allows to reduce significantly the Effective Material Losses (EML). In 2015, Islam *et al.* proposed a design based on a slotted porous core and obtained a configuration with a high birefringence equal to 7.5×10^{-2} at an operating frequency of 1 THz. Simultaneously, their configuration achieved low-loses [26]. Recently, a porous-core PCF, with elliptical holes in the core, was proposed [27]. In their study, the authors demonstrated that the ellipses rotation has a strong impact on the birefringence and the EML because it helps to break the symmetry of the fiber core. However, some crucial design issues for THz guidance, such as dispersion, confinement losses, and its application on the design of new compact devices were not considered. Another THz waveguide with elliptical holes in the core was proposed by Islam *et al.* [17]. In this work, they demonstrate that the anisotropic structure of elliptical air holes inside the core offers simultaneously high birefringence and low-effective material loss. In addition, they take advantage of this structure to design a sensor for measuring ethanol concentration [6] and a waveguide with potential application as a multichannel communication system [16].

On the other hand, other THz fiber devices, such as THz fiber filters, THz fiber couplers, and THZ polarization beam splitters (PBS) have also been proposed [28]–[31]. An all fiber-based polarization splitter is one of the most important devices in a THz system and, to design it effectively, the operational bandwidth and transmission loss properties are key considerations. Consequently, many configurations of PBS have been proposed using structures with rectangular cores with slots [28], dual-elliptical cores [30], and dual-core photonic crystal fiber with orthogonal microstructure [32]. All these configurations show the importance of the orientation of one core respect to the other. For this reason, PBS can be divided into symmetric and asymmetric coupler structures. In the former, the structure is based on two identical birefringent cores, while in the latter, the structure does not have identical cores. As expected, the behavior of these devices depends on the interaction of the field between both cores because both parallel and perpendicular polarizations

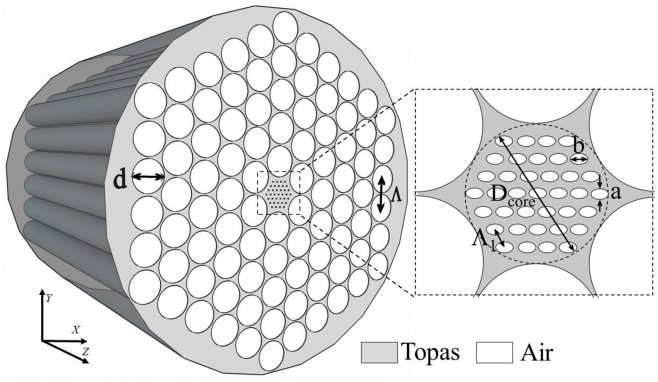

Fig. 1. Cross-section view of the proposed porous-core PCF with Elliptical Holes. The inset shows the enlarged view of the porous-core with a porosity of 80% when the elliptical holes are oriented at 0°.

can be coupled totally or partially between them, albeit at different coupling lengths. Thus, with the manipulation of the transmission length, the two polarizations can be easily separated [28], [30], [33]. In addition, the implementation of structures based on porous cores can help these devices to reduce the absorption losses and the dispersion effects.

In this paper, we present two THz polarization beam splitters based on a symmetric and an asymmetric fiber coupler structure. In the first section, we analyze the guided mode of a polymer THz waveguide based on a porous-core PCF with elliptical holes. The proposed configuration shows low-absorption loss and a maximum birefringence of 3×10^{-2} at 1 THz. Likewise, the proposed waveguide presents a dispersion flattened from 0.72 THz to 2 THz, where the variation of the dispersion coefficient is 0.37551 ± 0.1281 ps/THz/cm. Then, we use the same core structure to design a novel polarization beam splitter based on it. Two different configurations (symmetric and asymmetric) are evaluated to demonstrate that the device exhibits a strong polarization-dependent coupling behavior. The theoretical results with symmetric cores indicate that a 23 cm long splitter with a high Extinction Ratio (ER) greater than 90 dB and a narrow-bandwidth of 0.01 THz can be obtained at an operation frequency of 1.048 THz. We also study a directional coupler with asymmetric cores to be compared. In this case, the two polarizations can be totally coupled between the two cores with different coupling lengths. Simulation results shows that a 10.9 cm long splitter can be obtained with ultra-bandwidth of 0.306 THz (from 0.862 THz to 1.166 THz) and 0.23 THz (from 0.926 THz to 1.157 THz) for x- and y-polarization, respectively. This work includes details of the design of the subwavelength-scale air slot core, simulation results on the characteristics of the two dual-core polarization structures, a comparison between the two structures, as well as a discussion on the possible fabrication methods.

2. Design of Proposed Waveguide

Fig. 1 shows the schematic cross section of the proposed THz Photonic Crystal Fiber (PCF). The cladding region structure consists of a hexagonal lattice of circular holes. The diameter of each air hole in the cladding region is denoted as d, and Λ is the distance between two adjacent holes. In this case, the air-filling fraction (d/Λ), equal to 0.95, is kept fixed throughout all numerical calculations in order to guarantee a good confinement factor and flat dispersion properties. For the core region, we propose an arrangement with hexagonal distribution using thirty-seven elliptical holes. The diameter of the minor and major axes of the elliptical air holes are denoted by a and b, respectively, and the space between two adjacent elliptical air holes in the core is denoted as Λ_1. The porosity of the structure is defined as the fraction of the air holes to the core area, which depends on the distribution and size of the elliptical holes [13]. Then, to obtain the porosity of our waveguide, the value of Λ_1 is kept constant for each value of $D_{core} = 2(\Lambda\text{-d}/2)$, while the size of elliptical air-hole diameter changes to get different values of porosity at a particular value of D_{core}. Fig. 1 evidence

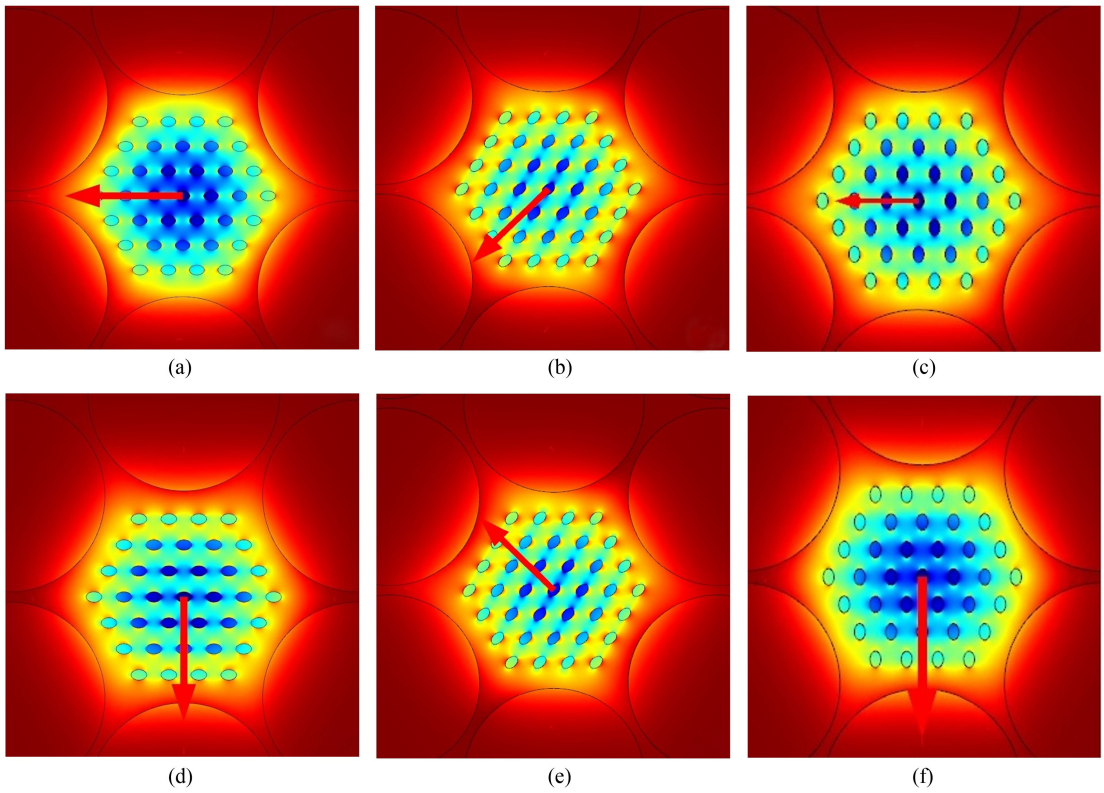

Fig. 2. Power flow distribution of the fundamental mode of the proposed THz-PCF at 1 THz and the $D_{core} = 400$ μm with different orientation of ellipses in the core region: (a), (d) $\theta = 0°$; (b), (e) $\theta = 45°$; (c), (f) $\theta = 90°$. Red arrows illustrate the directions of transverse electrical fields.

that D_{core} is the diameter of the core. In our design, we are employing $a = 19.6$ μm, $b = 29.4$ μm, $\Lambda_1 = 56.57$ μm, $\Lambda = 380.95$ μm and the total diameter of the waveguide was 4.27 mm. Using these parameters, the initial porosity is 80%. In addition, we perform the whole simulation using five rings of air holes in the cladding region and three rings of air holes in the core region.

The host material of the whole PCF is COC (Cyclic Olefin Copolymer, commercially known as TOPAS), as it provides significant advantages over other polymers. It has a refractive index of approximately 1.53 and material losses of 1 dB/cm, as shown in [34]. We also employ this material because the bulk material losses (α_{mat}) present a linear behavior from 0.1 THz to 2 THz. Furthermore, it is insensitive to humidity changes [7], [34].

Numerical analysis of the proposed THz-PCF was performed using COMSOL Multiphysics v.5.1, which is based on full-vectorial Finite Element Method (FEM). A circular Perfectly Matched Layer (PML) boundary condition was applied to absorb the scattered electromagnetic waves towards the surface [35]. The PML is the most efficient absorption boundary condition and its circular shape is defined in order to improve calculation modes in this type of structures [15], [36].The thickness of the PML is an important parameter due to its great impact on the simulation results. Therefore, we carry out the convergence test and found that the optimal results were obtained at a PML thickness above 9% of the total diameter. Fig. 2 depicts the transverse electric field distribution in the proposed THz fiber. The result shows the behavior of the E-field when the orientation angle of the elliptical holes is varied from 0° to 90°. This analysis was performed with $D_{core} = 400$ μm, a porosity of 80% and $f = 1$ THz. From these results, it is clear that the orientation of the E-field is aligned with the minor and major axes of the elliptical holes in all cases. Since there is a high birefringence induced by the geometric structure, this result could produce waveguides with a specific polarization in this region of the electromagnetic spectrum. The polarization is maintained all the way through the fiber

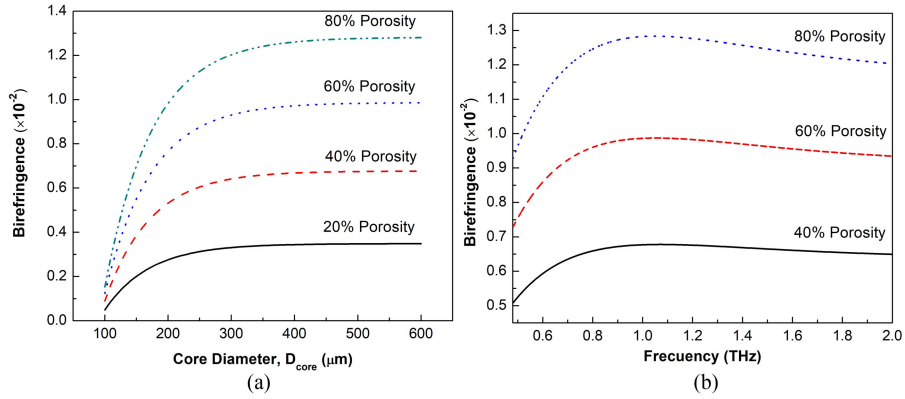

Fig. 3. (a) Birefringence as a function of D_{core} for different porosity values at 1 THz. (b) Birefringence as a function of frequency with $D_{core} = 400\ \mu$m for different porosity values.

like a PM optical fiber. Moreover, an increase in the energy density in the air-hole region of the core can be observed. This occurs as a consequence of the slot effect, which induces an increase of the electric field in the low refractive index region when the air holes (or slot region) have sub-wavelengths dimensions. This effect also helps to reduce the losses because energy propagates mostly in the core region [37].

3. Performance Characterization of the Proposed Terahertz Waveguide

The influence of the porosity on the birefringence for different values of D_{core} was evaluated to examine the performance of the proposed THz-PCF. The results are illustrated in Fig. 3(a). In this case, the porosity clearly has a great impact on the birefringence of the PCF, since the anisotropy of this structure increases as the porosity grows. Besides, we observed that the birefringence for all porosities remains almost constant with a D_{core} bigger than 350 μm. The maximum birefringence obtained for this design was 1.32×10^{-2}, which is bigger than the birefringence reported in ref. [16], [38], [39] and it has the same order of magnitude to the reported by [17], [40], [41]. The dependence of the birefringence as a function of the frequency was also studied from 0.48 THz to 2 THz and the results are illustrated in Fig. 3(b). It is observed that the fiber with larger core porosity provides higher birefringence. Therefore, a maximum birefringence of 1.32×10^{-2} is reached from $\approx$0.75 THz to $\approx$1.5 THz, when the porosity is 80% and D_{core} is 400 μm. In addition, Fig. 3(b) presents two different regions. In the first region, the birefringence increases with the frequency from 0.48 THz to 1.058 THz (from 625 μm to 283.6 μm). As it is evident, at 0.48 THz the wavelength is bigger than the D_{core}. Thus, it presents a larger evanescent field that interacts with the cladding, mainly because the core is virtually negligible. However, when the frequency increases, the wavelength decreases and the wave is affected by the anisotropy of the cladding and the core. On the other hand, a second region appears from 1.058 THz to 2 THz (from 283.6 μm to 150 μm). In this region, the results oppose those of the first one because in this case, the wavelength is always smaller than the D_{core}. As a consequence, the radiation is well confined in the core. Then, the birefringence only depends on the core asymmetry. Therefore, a slight decrease is presented. This anomalous behavior is more common in waveguides with a porous core [2], [41].

Since propagation loss is one of the main issues with waveguides in the THz region, the losses by absorption of the material and the confinement losses were analyzed in this work. The absorption losses are determined with the following expression [42]:

$$\alpha_{eff} = \sqrt{\frac{\varepsilon_0}{\mu_0}} \left(\frac{\int\int_{mat} n_{mat} \alpha_{mat} |\vec{E}|^2 dA}{|\int\int_{all} \vec{S}_z dA|} \right) \quad (1)$$

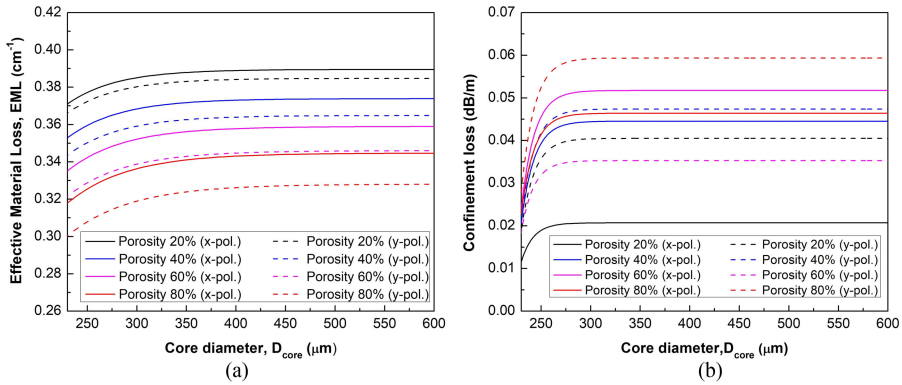

Fig. 4. (a) Effective material Loss as a function of D_{core} for different porosity cases at 1 THz. (b) Confinement losses as a function of D_{core} for different porosity cases at 1 THz.

where ε_0 and μ_0 are the permittivity and permeability in the vacuum, respectively; n_{mat} is the refractive index of the material; and α_{mat} is the bulk material absorption losses, which depend on the operating frequency [34], [43]. The results indicate that the EML can be reduced by increasing the core porosity, as shown in Fig. 4(a). This happens because a smaller portion of the material interacts with the THz waves in a high core porosity fiber. In addition, the EML depends on the polarization of the incident beam. The analysis of the EML was performed with $\theta = 0^\circ$. At this condition, there is an alignment with the major axis of the elliptical holes, as illustrated in Fig. 2. In addition, the confinement losses of the proposed waveguides were studied. To perform this analysis, different values of D_{core} and porosities were considered, while the ellipses orientation ($\theta = 0^\circ$) and the operating frequency (1 THz) remained constant. The results are illustrated in Fig. 4(b). The influence of the core porosity was evaluated, and small values were obtained in all cases. Additionally, confinement losses smaller than 0.06 dB/m for $D_{core} \geq 250$ μm were observed essentially constant in the studied range. In this case, confinement losses increase with the porosity, which evidence a strong contrast to the EML. We believe that a high core porosity provides low-index difference between the core and the cladding of the porous core PCF. Then, the confinement losses increase as the core porosity grows [15], [23], [40].

Another important parameter in THz-PCFs is the dispersion, because it limits the quality of the signal transmission on optical links. The dispersion effect can induce a pulse broadening, which causes inter-symbol interference among the different signals that travel simultaneously on the fiber [26], [41], [44].In addition, low dispersion and dispersion-flattened profile are particularly suitable for broadband signal transmission. The background material and the structural geometry might cause dispersion. In our case, the former is neglected because the refractive index of TOPAS is constant from 0.1 to 2 THz [43]. The waveguide dispersion can be calculated using the following expression:

$$\beta_2 = \frac{2}{c}\frac{dn_{eff}}{d\omega} + \frac{\omega}{c}\frac{d^2 n_{eff}}{d\omega^2}, \tag{2}$$

where ω is the angular frequency, c is the velocity of light in vacuum, n_{eff} is the effective index and f is the frequency. Thus, the dispersion as a function of the frequency was evaluated, and the results are illustrated in Fig. 5. It is clear that changes in the porosity and the polarization do not induce significant alterations on the dispersion behavior. Furthermore, the dispersion by the configuration with a porosity of 80% was calculated. In this case, the results suggest that our configuration has a flattened dispersion from 0.72 THz to 2 THz. To our knowledge, the flattened dispersion band is the longest reported to date. Here, the absolute variations of values of β_2 are less than 0.5 ps/THz/cm. Table 1 summarizes the results obtained for the different porosities analyzed. The β_2 and the flat band obtained in this work is better than the ones reported recently by other authors [39], [40], [45].

The fabrication process of a PCF is a tough, but a profitable challenge. However, fabrication precision and accuracy have been substantially improved thanks to the technological breakthrough

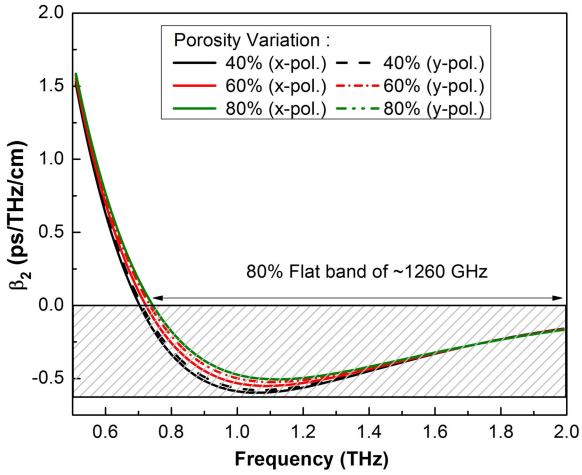

Fig. 5. Dispersion as function of the frequency for x-polarization and y-polarization at different porosities with $D_{core} = 400\ \mu$m.

TABLE 1
Dispersion and Bandwidth Comparison at Different Porosities

Porosity (%)	Polarization	Bandwidth (GHz)	Absolute variations of β_2 (ps/THz/cm)
40	x	1310	0.44823±0.1490
	y	1300	0.43432±0.1449
60	x	1279	0.41136±0.1395
	y	1272	0.38786±0.1362
80	x	1260	0.37551±0.1281
	y	1260	0.37551±0.1281

in recent years, which has made possible manufacturing structures that were very complex in the past, such as slots or elliptical holes. Due to that the core and cladding regions in our proposed waveguide have different structures, the best way of approaching the fabrication problem is by the implementation of different construction methods for each region, as was demonstrated by several research groups [22], [24], [46], [47]. In our case, we believe that the best approach is the technique based on stack and draw for the cladding circular lattice region, given that this technique has demonstrated to be a precise method for an efficient construction of a PCF with a hollow hexagonal lattice [14], [48], [49]. For the porous core, several proposed and proven techniques have been developed. Some of them are the extrusion technique [22], [24], [46], [50] and the versatile Sol-gel technique. Sol-gel is an interesting proposal since several PCF with different size holes have been constructed with this method [51]. Lastly, a new approach to the problem has appeared in the 3D printing. This method has proven to be successful in the design of Bragg structures and hollow-core fibers for THz frequencies [52], [53].Therefore, we believe that the proposed THz-PCF can be fabricated without major complications.

4. Terahertz Polarization Beam Splitter Based on the Proposed Fiber

In the previous section, we demonstrated that a porous-core PCF with elliptical holes could achieve high birefringence, flat dispersion, and low losses. Then, by extending the single core structure to a dual-core one, we can implement this fiber structure as a Terahertz Polarization Beam Splitter (PBS). Fig. 6(a) shows a schematic of the dual-core fiber with symmetric structure. In this case, the proposed PBS consists of two identical cores A and B. The structure is characterized because the cores have a $D_{core} = 400\ \mu$m, a porosity equal to 80%, $\Lambda = 380.95\ \mu$m and $d/\Lambda = 0.95$; the

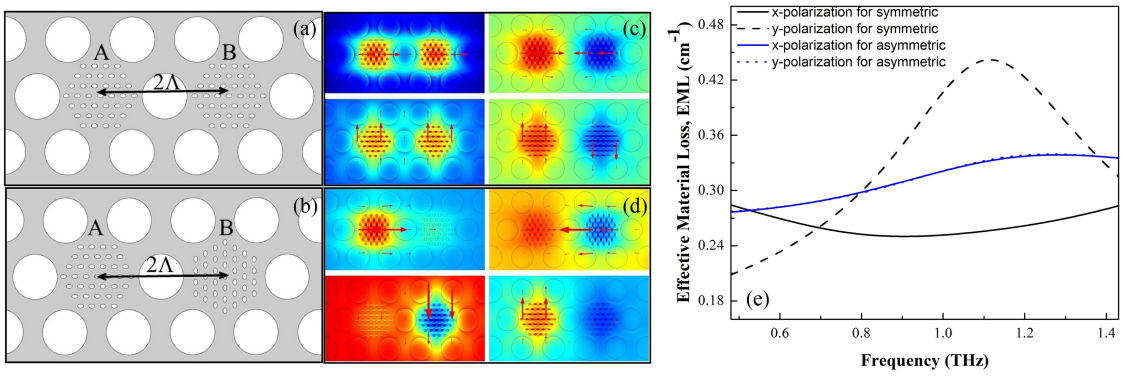

Fig. 6. (a) Cross-section and (b) electric field distributions of the four transmission super modes of the Polarization Beam Splitter with symmetric structure. (c) Cross-section and (d) electric field distributions of the four transmission super modes of the Polarization Beam Splitter with asymmetric structure. (e) Effective material absorption loss for the polarization beam splitters based on symmetric and asymmetric cores. The parameters of these structures are $D_{core} = 400$ μm, $\Lambda = 380.95$ μm, d/$\Lambda = 0.95$, porosity $= 80\%$, $a = 19.6$ μm, $b = 29.4$ μm at 1 THz.

distance between the two cores is 2Λ as it is illustrated in Fig. 6(a). The distance between both cores allows them to interact, and therefore there is coupling energy between them. Consequently, the coupling modes of each individual core will superpose into even and odd super modes, which have symmetric and antisymmetric electric field distributions as is shown in Fig. 6(b). This Figure shows the electric field distributions of the even and odd super modes for the x- and y-polarizations at 1.0 THz. Likewise, the PBS with symmetric structure presents a strong interaction for both polarizations because this structure has two identical cores.

In order to evaluate the influence of the symmetry structure on the performance of the PBS, we propose a second configuration with asymmetric structure as is illustrated in Fig. 6(c). The PBS with asymmetric configuration just differs because the air elliptical-holes in the core B are rotated 90 degrees, while the other parameters are fixed. Fig. 6(d) illustrates the electric field distribution of the even and odd super modes for both polarizations in the PBS with asymmetric structure. As it is evident, in this case, the coupling between both cores is very weak. Fig. 6(e) shows the EML as a function of the frequency of both PBS configurations studied in this work. It is clear that the configuration with asymmetric cores is better because the losses in both polarizations always have the same value within the study range, while the configuration with symmetric cores presents higher EML for y-polarization.

The performance and basic properties of the PBS can be analyzed by employing the coupled mode theory [54]. Therefore, the coupling behavior between both cores can be achieved by using a super mode analysis [48], [55]. The super modes are formed by modes of the individual cores. Thus, we can define this theory as the overlap of even and odd field distributions. This analysis requires that both even and odd super modes be excited simultaneously [54], [56]. Hence, the coupling length (L_c) is defined as the length of the fiber where a complete power transfer occurs between core A and core B . It is given by Eq. (3) [33], [55]

$$L_{c,i} = \frac{\lambda}{2(n^i_{even} - n^i_{odd})}, \tag{3}$$

where λ is the wavelength of incident light; n_{even} and n_{odd} are the effective refractive indices of even and odd supermodes, respectively; and i denotes the x- or y-polarization direction. COMSOL Multiphysics was used to obtain the n_{eff} of the four supermodes in both configurations. These values were employed to obtain the coupling lengths for x- and y polarizations. Usually, L_x and L_y are not equal. In other words, a complete power transfer for x and y polarization usually occurs at different lengths as a consequence of the high birefringence. Thus, for example, when it is analyzed the PBS with symmetric structure at 1 THz, we obtained $n^x_{even} = 1.36623$, $n^x_{odd} = 1.358397$,

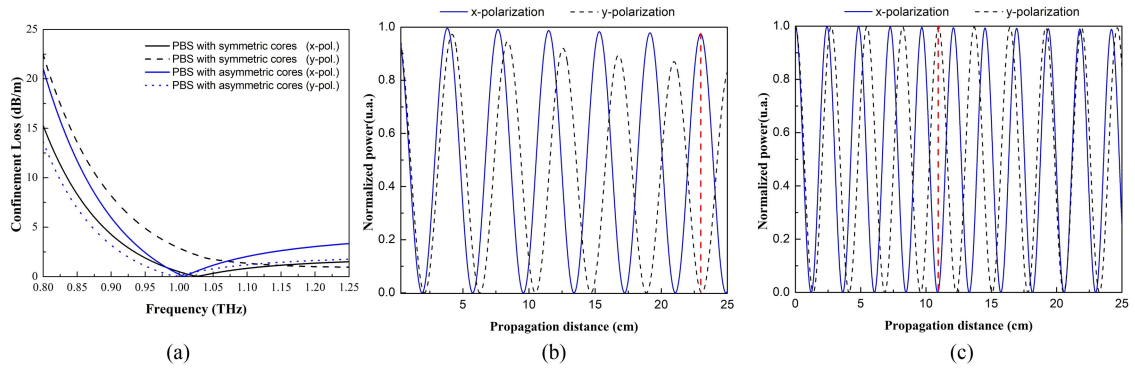

Fig. 7. (a) Confinement losses for both polarization beam splitters. Variations of the normalized power with the propagation distance at 1 THz. (b) Configuration with symmetric cores. (c) Configuration with asymmetric cores.

$n^{y}_{even} = 1.357085$ and $n^{y}_{odd} = 1.349934$. Then, the coupling lengths L_x and L_y can be easily obtained, which in this case, are 19.1472 mm and 20.9724 mm, respectively. Similarly, the coupling lengths by PBS with asymmetric configuration were $L_x = 12.0979$ mm and $L_y = 13.6907$ mm. Now, assuming that a fundamental mode with power P_{in} is launched into the core A, the normalized output power from core A and core B, $P_{out,A}$ and $P_{out,B}$, can be expressed as follows [28]:

For core A:

$$P^{i}_{out,A} = P^{i}_{in} Cos^2 \left(\frac{\pi Z}{2L_{c,i}} \right) e^{-\alpha^{i}_{loss} Z}, \tag{4}$$

For core B:

$$P^{i}_{out,B} = P^{i}_{in} Sin^2 \left(\frac{\pi Z}{2L_{c,i}} \right) e^{-\alpha^{i}_{loss} Z}, \tag{5}$$

where Z is the propagation length and α^{i}_{loss} is the confinement loss of the dual core fibers and it is considered as the average value of the confinement loss of the even and odd modes for the corresponding i-polarization. Note that the polarized light beam propagates in the fiber through the super mode coupling. Fig. 7(a) shows the confinement loss as a function of the frequency of both PBS configurations studied in this work. It is clear that the configuration with asymmetric cores is better because the confinement losses in both polarizations are aproximatly zero close to 1 THz, while the configuration with symmetric cores presents higher confinement losses for y-polarization. Figs. 7(b) and 7(c) show the normalized power at the output end in the core A as a function of the propagation distance for the PBS with symmetric and asymmetric configuration, respectively. Fig. 7(b) shows the normalized power for x and y-polarizations when assuming that the incident radiation is launched into the core A. We can observe in Fig. 7(b) that the power of each polarization mode changes periodically in core A. Consequently, it demonstrates that core A is coupling with core B. Moreover, the high birefringence in our design induces a difference between the coupling lengths. Therefore, the normalized output power of the x-polarization mode is out of phase with respect to the normalized output power of the y-polarization mode. On the one hand, both polarizations are effectively separated from each other by a distance of 23 cm (red dashed line in Fig. 7(b)) in the PBS with symmetric structure. Thus, for example, at 23 cm the output power for x- and y-polarization are 0.943475 and 2.619×10^{-3}, respectively, which is easily validated because this analysis was carried out at 1 THz. Then, as shown in Fig. 7(a), the confinement losses approximately are 0.113586 m^{-1} for x-polarization and 0.664202 m^{-1} for y-polarization. On the other hand, the PBS with asymmetric structure presents the maximum difference between both polarizations at 10.9 cm distance, as illustrated in Fig. 7(c). From these results, it is evident that the configuration with asymmetric cores has a better performance, since the device length is shorter than in the PBS based on symmetric cores.

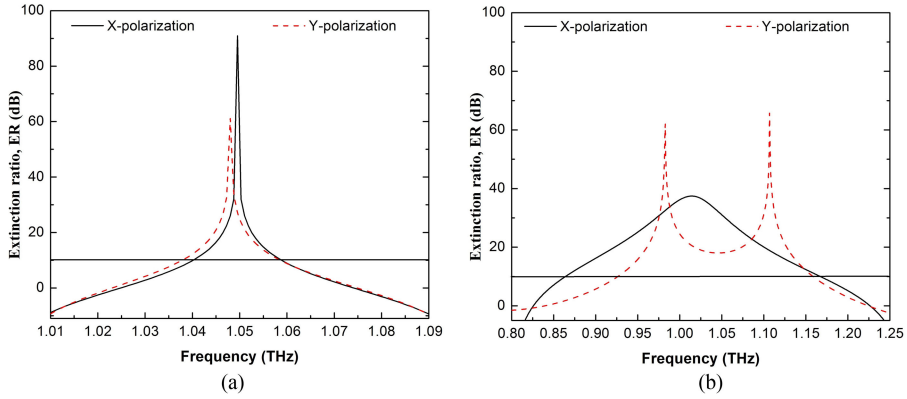

Fig. 8. Extinction ratio as function of the frequency. (a) PBS with symmetric cores. (b) PBS with asymmetric cores.

Finally, Extinction Ratio (ER) might be the most important parameter of a polarization beam splitter. This parameter is defined as the power ratio between the undesired and the desired polarization mode in each output core [28]. Thus, we can calculate this parameter for core A and core B by using the following equations [33]:

$$ER_x = 10Log_{10}\left(\frac{P_{out,y}}{P_{out,x}}\right), \tag{6}$$

$$ER_y = 10Log_{10}\left(\frac{P_{out,x}}{P_{out,y}}\right), \tag{7}$$

where $P_{out,x}$ and $P_{out,y}$ are the output powers of the x- and y-polarization at the output end of the left core. Only when ER is lower than -10 dB or higher than 10 dB, it is possible to guarantee that the two different polarization states are completely separated. Fig. 8 shows the variations of the ER in function of the frequency for the PBS with symmetric cores and asymmetric structures. On the one hand, Fig. 8(a) shows the results obtained by the PBS with symmetric cores. It presents an ER higher than 90.8 dB at $\approx$1.049 THz for x-polarization, while the ER for y-polarization just reached 61 dB at 1.048 THz. Fig. 8(a) evidences that the PBS with symmetric structure has a narrow bandwidth ($\approx$0.01 THz) for both polarizations. On the other hand, the results obtained by the PBS with asymmetric structure show a significant increase in the bandwidth for both polarizations compared with the symmetric one. Fig. 8(b) shows that this configuration has a bandwidth of 0.306 THz (from 0.862 THz to 1.166 THz) in x-polarization and of 0.231 THz (from 0.926 THz to 1.157 THz) in y-polarization. On the other hand, the ER by y-polarization presents two peaks; it is due to the fact that the output power is zero at 0.9828 THZ and 1.0684 THz, and consequently ER$\longrightarrow\infty$ in the PBS with asymmetric cores. The two PBS configurations proposed in this work present a better performance than others reported in the past [28], [30]–[32]. For example, the proposed PBS presents a bandwidth 15.3 times higher than the one proposed by Chen *et al.* [30] and 1.7 times higher than the proposed by Chen *et al.* [28].

5. Conclusions

A novel design of a THz-PCF was proposed and analyzed with the full-vector Finite Element Method. The proposed design was based on the combination of two different structures: one structure had elliptical holes in the core and the other one had circular holes in the cladding region. The obtained results demonstrated that this fiber could be used as a waveguide because it had smaller losses than other proposed configurations. Furthermore, the results indicated that when adjusting the structural parameters appropriately, a high birefringence, low-losses and low-dispersion properties could be easily achieved within the frequency range from 0.5 THz to 2 THz. Additionally, the analysis of

dispersion demonstrated that our configuration with an 80% porosity exhibited a flattened dispersion in the frequency range from 0.72 THz to 2 THz and the variation of the dispersion coefficient within this range was 0.37551 $\pm$ 0.1281 ps/THz/cm.

Finally, the proposed fiber was used to design two types of THz polarization splitters. Two different polarization-splitting mechanisms, with symmetric cores and asymmetric cores, were numerically studied and compared. We found that the configuration with asymmetric cores presented a better performance because it allowed to operate in an ultra-wide band (from 0.862 THz to 1.166 THz) and the device length was shorter (10.9 cm) than in the symmetric one. The configuration with symmetric cores presented a higher extinction ratio (close to 1.049 THz by x-polarization). In conclusion, we demonstrated that the behavior of the PBS depended on the polarization, the core structure, and the operation frequency. The proposed fiber could be used in THz sensing, telecommunications, medical diagnostic images, and spectroscopy applications.

Acknowledgement

The authors would like to thank the anonymous reviewers for their valuable suggestions.

References

[1] T. Ouchi *et al.*, "Terahertz imaging system for medical applications and related high efficiency terahertz devices," *J. Infrared, Millimeter, Terahertz Waves*, vol. 35, no. 1, pp. 118–130, 2014.
[2] J. Sultana, M. Islam, M. Islam, and D. Abbott, "High numerical aperture, highly birefringent novel photonic crystal fibre for medical imaging applications," *Electron. Lett.*, vol. 54, no. 2, pp. 61–62, Jan. 2018. [Online]. Available: http://digital-library.theiet.org/content/journals/10.1049/el.2017.3694
[3] M. Tonouchi, "Cutting-edge terahertz technology," *Nature Photon.*, vol. 1, no. 2, pp. 97–105, 2007.
[4] D. Mittleman, *Sensing With Terahertz Radiation*. New York, NY, USA: Springer, 2003.
[5] M. S. Islam *et al.*, "A novel approach for spectroscopic chemical identification using photonic crystal fiber in the terahertz regime," *IEEE Sensors J.*, vol. 18, no. 2, pp. 575–582, Jan. 2018. [Online]. Available: http://ieeexplore.ieee.org/document/8115280/
[6] J. Sultana, M. S. Islam, K. Ahmed, A. Dinovitser, B. W.-H. Ng, and D. Abbott, "Terahertz detection of alcohol using a photonic crystal fiber sensor," *Appl. Opt.*, vol. 57, no. 10, pp. 2426–2433, Apr. 2018. [Online]. Available: https://www.osapublishing.org/abstract.cfm?URI=ao-57-10-2426
[7] S. Koenig *et al.*, "Wireless sub-THz communication system with high data rate," *Nature Photon.*, vol. 7, no. 12, pp. 977–981, Dec. 2013. [Online]. Available: http://www.nature.com/articles/nphoton.2013.275
[8] A. Barh, B. P. Pal, G. P. Agrawal, R. K. Varshney, and B. M. Rahman, "Specialty fibers for terahertz generation and transmission: A Review," *IEEE J. Sel. Topics Quantum Electron.*, vol. 22, no. 2, Mar./Apr. 2016, Art. no. 8500215.
[9] M. Beresna, M. Gecevičius, and P. G. Kazansky, "Ultrafast laser direct writing and nanostructuring in transparent materials," *Adv. Opt. Photon.*, vol. 6, no. 3, pp. 293–339, Sep. 2014. [Online]. Available: https://www.osapublishing.org/aop/abstract.cfm?uri=aop-6-3-293
[10] K. Wang and D. M. Mittleman, "Metal wires for terahertz wave guiding," *Nature*, vol. 432, no. 7015, pp. 376–379, Nov. 2004. [Online]. Available: http://www.nature.com/articles/nature03040
[11] C.-H. Lai, Y.-C. Hsueh, H.-W. Chen, Y.-J. Huang, H.-C. Chang, and C.-K. Sun, "Low-index terahertz pipe waveguides," *Opt. Lett.*, vol. 34, no. 21, pp. 3457–3459, Nov. 2009. [Online]. Available: https://www.osapublishing.org/abstract.cfm?URI=ol-34-21-3457
[12] M. Frankel, S. Gupta, J. Valdmanis, and G. Mourou, "Terahertz attenuation and dispersion characteristics of coplanar transmission lines," *IEEE Trans. Microw. Theory Techn.*, vol. 39, no. 6, pp. 910–916, Jun. 1991. [Online]. Available: http://ieeexplore.ieee.org/document/81658/
[13] S. Atakaramians, S. Afshar V., T. M. Monro, and D. Abbott, "Terahertz dielectric waveguides," *Adv. Opt. Photon.*, vol. 5, no. 2, pp. 169–215, Jun. 2013. [Online]. Available: https://www.osapublishing.org/aop/abstract.cfm?uri=aop-5-2-169
[14] P. Russell, "Photonic crystal fibers," *Science*, vol. 299, no. 5605, pp. 358–362, Jan. 2003. [Online]. Available: http://www.sciencemag.org/cgi/doi/10.1126/science.1079280
[15] E. Reyes-Vera, J. Usuga-Restrepo, J. Botero-Cadavid, and J. Zuñiga, "Design of low loss photonic crystal fiber based on porous-core with elliptical holes in THz regime," in *Proc. 3rd Int. Conf. Appl. Opt. Photon.*, Aug. 2017, Art. no. 237. [Online]. Available: https://www.spiedigitallibrary.org/conference-proceedings-of-spie/10453/2276427/Design-of-low-loss-photonic-crystal-fiber-based-on-porous/10.1117/12. 2276427.full
[16] M. S. Islam *et al.*, "Zeonex-based asymmetrical terahertz photonic crystal fiber for multichannel communication and polarization maintaining applications," *Appl. Opt.*, vol. 57, no. 4, pp. 666–672, Feb. 2018. [Online]. Available: https://www.osapublishing.org/abstract.cfm?URI=ao-57-4-666
[17] M. S. Islam, J. Sultana, A. Dinovitser, B. W. Ng, and D. Abbott, "A novel Zeonex based oligoporous-core photonic crystal fiber for polarization preserving terahertz applications," *Opt. Commun.*, vol. 413, pp. 242–248, Apr. 2018. [Online]. Available: https://doi.org/10.1016/j.optcom.2017.12.061http://linkinghub

[18] E. Reyes-Vera, E. Gonzalez-Valencia, and P. Torres, "Understanding the birefringence effects in an all-fiber device based on photonic crystal fibers with integrated electrodes," *Photon. Lett. Poland*, vol. 2, no. 4, pp. 168–170, Dec. 2010. [Online]. Available: http://photonics.pl/PLP/index.php/letters/article/view/160
[19] L.-J. Chen, H.-W. Chen, T.-F. Kao, J.-Y. Lu, and C.-K. Sun, "Low-loss subwavelength plastic fiber for terahertz waveguiding," *Opt. Lett.*, vol. 31, no. 3, pp. 308–310, 2006. [Online]. Available: https://www.osapublishing.org/ol/abstract.cfm?uri=ol-31-3-308
[20] J. Yang, B. Yang, Z. Wang, and W. Liu, "Design of the low-loss wide bandwidth hollow-core terahertz inhibited coupling fibers," *Opt. Commun.*, vol. 343, pp. 150–156, May 2015. [Online]. Available: http://linkinghub.elsevier.com/retrieve/pii/S0030401815000255
[21] L. Vincetti, "Single-mode propagation in triangular tube lattice hollow-core terahertz fibers," *Opt. Commun.*, vol. 283, no. 6, pp. 979–984, Mar. 2010. [Online]. Available: http://linkinghub.elsevier.com/retrieve/pii/S0030401809011547
[22] H. Bao, K. Nielsen, H. K. Rasmussen, P. U. Jepsen, and O. Bang, "Fabrication and characterization of porous-core honeycomb bandgap THz fibers," *Opt. Exp.*, vol. 20, no. 28, pp. 29507–29517, 2012. [Online]. Available: https://www.osapublishing.org/oe/abstract.cfm?uri=oe-20-28-29507
[23] S. Atakaramians, S. Afshar V., B. M. Fischer, D. Abbott, and T. M. Monro, "Porous fibers: A novel approach to low loss THz waveguides," *Opt. Exp.*, vol. 16, no. 12, pp. 8845–8854, 2008.
[24] S. Atakaramians *et al.*, "THz porous fibers: Design, fabrication and experimental characterization," *Opt. Exp.*, vol. 17, no. 16, pp. 14053–14062, Aug. 2009.
[25] K. Nielsen, H. K. Rasmussen, P. U. Jepsen, and O. Bang, "Porous-core honeycomb bandgap THz fiber," *Opt. Lett.*, vol. 36, no. 5, pp. 666–668, Mar. 2011. [Online]. Available: https://www.osapublishing.org/abstract.cfm?URI=ol-36-5-666
[26] R. Islam, G. Hasanuzzaman, M. S. Habib, S. Rana, and M. Khan, "Low-loss rotated porous core hexagonal single-mode fiber in THz regime," *Opt. Fiber Technol.*, vol. 24, pp. 38–43, Aug. 2015. [Online]. Available: http://linkinghub.elsevier.com/retrieve/pii/S1068520015000589
[27] S. Rana, M. Saiful Islam, M. Faisal, K. C. Roy, R. Islam, and S. F. Kaijage, "Single-mode porous fiber for low-loss polarization maintaining terahertz transmission," *Opt. Eng.*, vol. 55, no. 7, 2016, Art. no. 076114. [Online]. Available: http://opticalengineering.spiedigitallibrary.org/article.aspx?doi=10.11 17/1.OE.55.7.076114
[28] H. Chen, G. Yan, E. Forsberg, and S. He, "Terahertz polarization splitters based on total and partial coupling in dual slotted core polymer fiber: Comparison and analysis," *IEEE Photon. J.*, vol. 9, no. 3, Jun. 2017, Art. no. 7103315.
[29] J. Zi *et al.*, "Terahertz polarization converter based on all-dielectric high birefringence metamaterial with elliptical air holes," *Opt. Commun.*, vol. 416, pp. 130–136, Jun. 2018.
[30] H. Chen, G. Yan, E. Forsberg, and S. He, "Terahertz polarization splitter based on a dual-elliptical-core polymer fiber," *Appl. Opt.*, vol. 55, no. 23, pp. 6236–6242, Aug. 2016. [Online]. Available: https://www.osapublishing.org/abstract.cfm?URI=ao-55-23-6236
[31] Y. F. Zhu, M. Y. Chen, H. Wang, H. B. Yao, Y. K. Zhang, and J. C. Yang, "Design and analysis of a low-loss suspended core terahertz fiber and its application to polarization splitter," *IEEE Photon. J.*, vol. 5, no. 6, Dec. 2013, Art. no. 7101410.
[32] S. Li, H. Zhang, Y. Hou, J. Bai, W. Liu, and S. Chang, "Terahertz polarization splitter based on orthogonal microstructure dual-core photonic crystal fiber," *Appl. Opt.*, vol. 52, no. 14, pp. 3305–3310, May 2013.
[33] E. Reyes-Vera, F. Gomez, J. Usuga-Restrepo, and N. Gomez-Cardona, "Novel multiband polarization beam splitter based on a dual-core transversally chirped microstructured optical fiber," in *Proc. 3rd Int. Conf. Appl. Opt. Photon.*, Aug. 2017, Art. no. 229. [Online]. Available: https://www.spiedigitallibrary.org/conference-proceedings-of-spie/10453/2276381/Novel-multiband-polarization-beam-splitter-based-on-a-dual-core/10.11 17/12.2276381.full
[34] K. Nielsen, H. K. Rasmussen, A. J. Adam, P. C. Planken, O. Bang, and P. U. Jepsen, "Bendable, low-loss Topas fibers for the terahertz frequency range," *Opt. Exp.*, vol. 17, no. 10, pp. 8592–8601, 2009. [Online]. Available: https://www.osapublishing.org/oe/abstract.cfm?uri=oe-17-10-8592
[35] K. Saitoh and M. Koshiba, "Numerical modeling of photonic crystal fibers," *J. Lightw. Technol.*, vol. 23, no. 11, pp. 3580–3590, Nov. 2005.
[36] E. Reyes-Vera and P. Torres, "Influence of filler metal on birefringent optical properties of photonic crystal fiber with integrated electrodes," *J. Opt.*, vol. 18, no. 8, Aug. 2016, Art. no. 085804. [Online]. Available: http://stacks.iop.org/2040-8986/18/i=8/a=085804?key=crossref.68d51b9d44 f63d6c6c3962bfd65b0ac6
[37] G. S. Wiederhecker *et al.*, "Field enhancement within an optical fibre with a subwavelength air core," *Nature Photon.*, vol. 1, no. 2, pp. 115–118, 2007. [Online]. Available: http://opus.bath.ac.uk/8596/
[38] J. Tang, Z. Zhang, D. Luo, M. Chen, and H. Chen, "High birefringence terahertz photonic crystal fiber," *Opt. Eng.*, vol. 52, no. 1, 2013, Art. no. 014004. [Online]. Available: http://opticalengineering.spiedigitallibrary.org/article.aspx?doi=10.1117/1.OE.52.1.014004
[39] M. S. Islam, M. Faisal, and S. M. Razzak, "Dispersion flattened porous-core honeycomb lattice terahertz fiber for ultra low loss transmission," *IEEE J. Quantum Electron.*, vol. 53, no. 6, Dec. 2017, Art. no. 8500608.
[40] Z. Wu *et al.*, "Design of highly birefringent and low-loss oligoporous-core thz photonic crystal fiber with single circular air-hole unit," *IEEE Photon. J.*, vol. 8, no. 6, Dec. 2016, Art. no. 4502711.
[41] R. Islam, M. S. Habib, G. K. M. Hasanuzzaman, R. Ahmad, S. Rana, and S. F. Kaijage, "Extremely high-birefringent asymmetric slotted-core photonic crystal fiber in THz regime," *IEEE Photon. Technol. Lett.*, vol. 27, no. 21, pp. 2222–2225, Nov. 2015.
[42] G. K. Hasanuzzaman, M. Selim Habib, S. M. Abdur Razzak, M. A. Hossain, and Y. Namihira, "Low loss single-mode porous-core kagome photonic crystal fiber for THz wave guidance," *J. Lightw. Technol.*, vol. 33, no. 19, pp. 4027–4031, Oct. 2015.
[43] Y.-S. Jin, G.-J. Kim, and S.-G. Jeon, "Terahertz dielectric properties of polymers," *J. Korean Phys. Soc.*, vol. 43, no. 8, pp. 513–517, 2006.
[44] A. F. Betancur-Pérez, J. F. Botero-Cadavid, E. Reyes-Vera, and N. Gómez-Cardona, "Hexagonal photonic crystal fiber behaviour as a chromatic dispersion compensator of a 40 Gbps link," *Int. J. Electron. Telecommun.*, vol. 63, no. 1, pp. 93–98, Jan. 2017. [Online]. Available: http://www.degruyter.com/view/j/eletel.2017.63.issue-1/eletel-2017-0013/eletel-2017-0013.xml

[45] M. R. Hasan, S. Akter, T. Khatun, A. A. Rifat, and M. S. Anower, "Dual-hole unit-based kagome lattice microstructure fiber for low-loss and highly birefringent terahertz guidance," *Opt. Eng.*, vol. 56, no. 4, Apr. 2017, Art. no. 043108. [Online]. Available: http://opticalengineering.spiedigitallibrary.org/article.aspx?doi=10.11 17/1.OE.56.4.043108
[46] H. Ebendorff-Heidepriem and T. M. Monro, "Extrusion of complex preforms for microstructured optical fibers," *Opt. Exp.*, vol. 15, no. 23, pp. 15086–15092, 2007. [Online]. Available: https://www.osapublishing.org/oe/abstract.cfm?uri=oe-15-23-15086
[47] A. Dupuis, A. Mazhorova, F. Désévédavy, M. Rozé, and M. Skorobogatiy, "Spectral characterization of porous dielectric subwavelength THz bers fabricated using a microstructured molding technique," *Opt. Exp.*, vol. 18, no. 13, pp. 13813–13828, Jun. 2010. [Online]. Available: https://www.osapublishing.org/oe/abstract.cfm?uri=oe-18-13-13813
[48] E. Reyes-Vera, J. Úsuga-Restrepo, M. Varon, and P. Torres, "Dual-Core transversally chirped microstructured optical fiber for mode-converter device and sensing application," in *Selected Topics on Optical Fiber Technologies and Applications*. London, U.K.: InTech, Feb. 2018. [Online]. Available: http://www.intechopen.com/books/selected-topics-on-optical-fiber-technologies-and-applications/dual-core-transversally-chirped-microstructured-optical-fiber-for-converter-device-and-sensing-
[49] A. Méndez and T. F. Morse, *Specialty Optical Fibers Handbook*, E. Inc, Ed. San Diego, CA, USA: Academic, 2007.
[50] M. Mignanelli, K. Wani, J. Ballato, S. Foulger, and P. Brown, "Polymer microstructured fibers by one-step extrusion," *Opt. Exp.*, vol. 15, no. 10, pp. 6183–6189, 2007.
[51] R. Bise and D. Trevor, "Sol-gel derived microstructured fiber: fabrication and characterization," in *Proc. OFC/NFOEC Tech. Digest. Opt. Fiber Commun. Conf.*, 2005., vol. 3, pp. 11–13.
[52] A. L. Cruz, A. Argyros, X. Tang, C. M. Cordeiro, and M. A. Franco, "3D-printed terahertz Bragg fiber," in *Proc. 40th Int. Conf. Infrared, Millimeter, Terahertz Waves*, Aug. 2015, pp. 3–5.
[53] A. L. Cruz *et al.*, "3D printed hollow core fiber with negative curvature for terahertz applications," *J. Microw., Optoelectron. Electromagn. Appl.*, vol. 14, pp. SI45–SI53, 2015.
[54] D. L. Lee, *Electromagnetic Principles of Integrated Optics*, 1st ed. Hoboken, NJ, USA: Wiley, 1986. [Online]. Available: https://books.google.com.co/books?id=GOJRAAAAMAAJ
[55] E. Reyes-Vera, J. Úsuga-Restrepo, J. Acevedo-Echeverry, N. Gómez-Cardona, and M. Varón, "Performance analysis of a modal converter based on an asymmetric dual-core photonic crystal fiber," *Optica Pura y Aplicada*, vol. 50, no. 3, pp. 251–257, 2017. [Online]. Available: http://www.sedoptica.es/Menu_Volumenes/Pdfs/OPA_50_3_49023. pdf
[56] L. Szostkiewicz, M. Napierala, A. Ziolowicz, A. Pytel, T. Tenderenda, and T. Nasilowski, "Cross talk analysis in multicore optical fibers by supermode theory," *Opt Lett.*, vol. 41, no. 16, pp. 3759–3762, Aug. 2016. [Online]. Available: https://www.osapublishing.org/abstract.cfm?URI=ol-41-16-3759